Hindawi
Journal of Applied Mathematics
Volume 2022, Article ID 6875240, 11 pages
https://doi.org/10.1155/2022/6875240

Research Article

Comparison of the Flow Fields between Nozzles with Full-Open and Open-Close Valves at Transonic Velocity

Zijie Li and Hao Wang

Nanjing University of Science and Technology, School of Energy and Power Engineering, Nanjing 210094, China

Correspondence should be addressed to Zijie Li; 806287197@qq.com

Received 14 May 2022; Revised 29 August 2022; Accepted 27 October 2022; Published 30 November 2022

Academic Editor: Dan Huang

At transonic velocity, ejector nozzles require third auxiliary intake valves to increase air intake, resulting in good thrust performance. However, different intake structures will inevitably lead to different internal flow-field structures and thrust performances. To evaluate the differences between nozzles with full-open valve and open-close valve at transonic velocity, we established two numerical simulation models to analyze the flow-field structure and thrust performance in the ejector nozzle. The results show that at the transonic flight state (Ma = 1.2), the mainstream of the two models always maintains an overexpansion state, and the primary flow fields are highly similar. However, the secondary and the third auxiliary flow fields are significantly different. Notably, in the nozzle with open-close valve, a lateral flow occurs near the wall of the nozzle tail, resulting in several vortexes. Contrarily, in the nozzle with full-open valve, there is almost no lateral flow or vortex. Further, we found that the secondary flow tends to roll up toward the third auxiliary valve instead of directly flowing into the nozzle. Thus, the thrust coefficients of the two nozzles differ.

1. Introduction

In recent years, the turbine-based combined cycle engine has become a research hotspot in the aerospace field, and the injector nozzle based on the integration of intake and exhaust is one of the important components to realize the operation of the aircraft in a wide-speed range [1, 2]. With the research advancement on ejectors, revealing the ejection phenomenon and exploring its internal flow mechanism have become the main route to further improve the ejection efficiency [3, 4].

A typical and well-known engine with a multichannel injector nozzle is the J58 engine on the SR-71 aircraft, which is the key to the SR-71's excellent performance [5, 6]. At different Mach numbers, the opening states of each intake passage are different. That is, from Ma0 to Ma0.5, the airflow inside the engine is increased by inhaling from the outside through the valves on the side and front of the center body of the inlet. At this time, the intake valve of the nozzle is also in an open state, causing the ambient air exits the engine together with the upstream airflow. From Ma0.5 to Ma2.5, the open valve causes the resistance of the inhaled ambient airflow to balance the secondary flow. After Ma2.2, the valve in the closed state results in no suction from the outside, and the cooling air is discharged together with the primary flow [7–9].

Many studies on the flow-field structure of ejector nozzles have been conducted. Rao et al. [10] aim to compare and study the external and internal flow characteristics of an axisymmetric circular convergent nozzle, a nonsnake convergent nozzle with an elliptical outlet, and a shallow single serpentine convergent nozzle with an elliptical outlet under fully expanded conditions. The wall pressure measurement shows that, due to the axisymmetric shape, the traditional circular nozzle shows a symmetrical jet development. However, the flow through the serpentine nozzle makes the flow through it asymmetrical.

Harroun et al. [11] conducted computational and experimental research on the geometry of three nozzles, including a nozzleless blunt body typically and two aerospike nozzles of RDE burners. The results show that the effect of the high momentum increased by the highest pressure knock product

on the exhaust plume is different from the comparable steady flow field supplied by the same average product gas flow rate.

Luginsland [12] conducted a numerical study on the influence of nozzle geometry; namely, nozzle wall thickness and nozzle length on the vortex breakdown of a compressible, swirling nozzle jet. The results presented again emphasize the important role played by the upstream nozzle configuration.

Wu and Dong [13, 14] designed an adjustable nozzle that can adapt to the airflow by changing the outlet area of the ejector nozzle under different inflow conditions. The auxiliary intake valve is added on the basis of ejector nozzle model, which can automatically adjust the expansion degree of the mainstream according to the fluid state to prevent the airflow from overexpanding.

Deng et al. [15] designed several sets of ejector nozzle models with different geometric parameters for numerical research. The results show that when the secondary flow is in the choke state (the secondary flow channel is closed), the thrust coefficient of the ejector nozzle increases with the increase of the outlet area. When not in a choke state, the flow coefficient of the secondary flow increases as the outlet area becomes larger. Meanwhile, the nozzle thrust coefficient is determined by the outlet area and the mainstream pressure ratio.

From the above, it is clear that most of the researches on the ejector nozzle mainly focus on analyzing the influence of the external and internal flows of the nozzle at supersonic velocities. However, there are a few reports on the analysis of the vortex characteristics in the ejector nozzle with an open-close auxiliary valve at transonic velocities. In fact, the open-close auxiliary valve changes the flow phenomenon inside the nozzle; thus, a related numerical simulation study appears to be of great significance.

One key feature of this work is that the flight state is transonic (Ma = 1.2). In a high Mach state (Mach number is >1.5), owing to the relatively large primary nozzle pressure ratio, the auxiliary intake valve closes, i.e., there is no third auxiliary airflow. Meanwhile, the tail nozzle rotates outward until it is horizontal. In contrast, the flow state in the nozzle is relatively simple; i.e., only mixing and energy transfer between the primary flow and the secondary flow occur.

However, in the sub-/transonic state, there are three airflows to increase the thrust performance of the nozzle. The three airflows still interfere with each other, particularly the secondary and third auxiliary flows. Therefore, the difference between this study and previous studies is that here, a strong coupling interference is formed when the auxiliary valve opens, which increases the complexity of the flow-field structure. Especially when the auxiliary intake valve is of open-close structure, a lateral flow will be generated in the nozzle, resulting in the appearance of multiple pairs of vortexes, which can improve the thrust performance of the nozzle.

This paper is organized as follows. Section 2 details the physical models, and provides further details regarding the simulation domain sizes and meshes, as well as the structure of the ejector nozzle. In Section 3, the simulation results of the ejector nozzle are discussed regarding the performance analysis and the flow-field structure. Section 4 provides conclusions.

2. Physical Model and Mesh Model

2.1. Physical Model. The ejector nozzle designed in this paper involves three airflows; namely, the primary flow, the secondary flow, and the third auxiliary flow. The secondary flow gas comes from the air inlet while the third auxiliary flow is the ambient gas of the aircraft outer body naturally inhaled. The secondary stream and the third auxiliary stream will mix with the main stream ejected from the primary nozzle and flow out of the ejector nozzle together. The research focus of this paper is to analyze the influence on the intake state of the third auxiliary flow, so the structure of the injector nozzle is simplified. Figures 1(a) and 1(b) show the schematic diagrams of the 3-D physical model of the ejector nozzle. The model mainly includes four parts: the primary nozzle, secondary nozzle, third auxiliary valve, and tail nozzle. Among them, the third auxiliary valve in Figure 1(a) is an interval type; i.e., half of the valve is open to suck in the external flow, whereas the other half is closed and cannot take in the external flow, thus forming the open-close alternate intake valve. Conversely, the third auxiliary valve of the nozzle model in Figure 1(b) is fully open.

Figure 2 shows the schematic diagram of the 2-D structure parameters of the ejector nozzle. Among them, the outlet area adjustment piece at the tail of the ejector nozzle is folded inward to reduce the outlet area and avoid serious overexpansion of the primary flow. In addition, the width of the closed valve is 100 mm, which is the same for the open valve. Table 1 shows the specific values of each parameter.

2.2. Meshing Method. The 3-D ejector nozzle involved in this study has a symmetrical, span-wise periodic structure. To save calculation time and cost, we simulated the ejector nozzle structure in the upper half of a single cycle, as shown in Figure 3. The whole computational domain is divided by structural grids, with a total of 7 million grids. Furthermore, to avoid boundary pollution caused by the extremely small calculation domain, the computational domain is large enough with a length of about 1900 mm in the airflow direction, a width of about 600 mm, and 600 mm in height. Additionally, all the walls and nozzle outlets had been subjected to local mesh densification. Furthermore, we refined the grid at the wall, setting the height of the first layer of the wall to 0.05 mm.

Figure 4 shows the boundary types of the nozzle model. We adopted the free incoming flow as the pressure far-field boundary; correspondingly, the outlet of the calculation domain and nozzle adopted the pressure-outlet boundary condition. All object surfaces were set as nonslip insulating wall. For the nozzle, the inlet of the primary nozzle and the inlet of the secondary nozzle adopted the pressure-inlet boundary condition. In the simulation process, the total inlet pressure and static temperature were specified. The values of the corresponding boundary parameters are listed in Table 2. Basically, the incoming flow Mach number is 1.2,

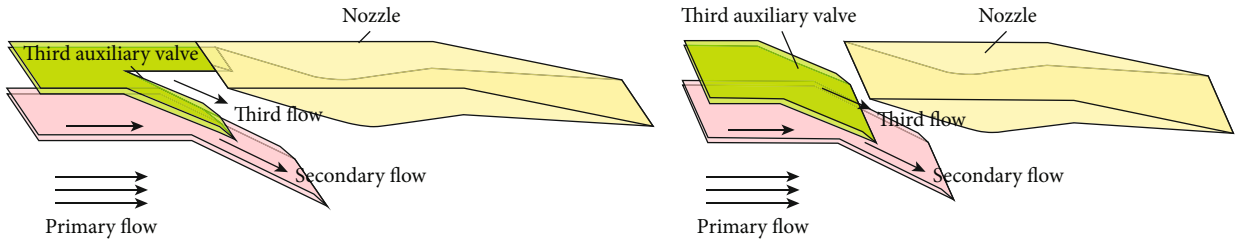

(a) Physical model of nozzle with open-close valve

(b) Physical model of nozzle with full-open valve

Figure 1: Three-dimensional physical model of the ejector nozzle.

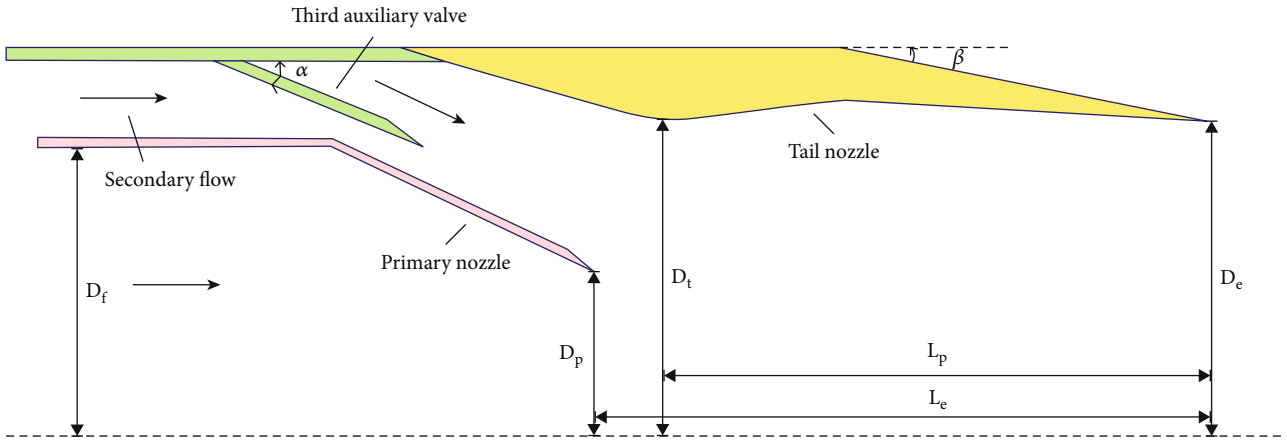

Figure 2: Two-dimensional physical structure parameters of an ejector nozzle.

Table 1: Physical structure size parameters of an ejector nozzle.

Parameters	Values
Primary nozzle height (D_f)	120.75 mm
Secondary nozzle height (D_s)	40.38 mm
Primary nozzle outlet height (D_p)	55.75 mm
Throat height (D_t)	135.00 mm
Nozzle outlet height (D_e)	241.30 mm
Third auxiliary valve opening angle (α)	22°
Tail nozzle rotation angle (β)	11.5°
Distance from the tail nozzle outlet to the nozzle throat (L_p)	272.33 mm
Distance from the tail nozzle outlet to the primary nozzle outlet (L_e)	314.49 mm
Length of the third auxiliary valve (L_t)	98.2 mm
Width of the open valve (L_o)	100 mm
Width of the closed valve (L_c)	100 mm

ambient pressure is 30,800 Pa, and ambient temperature is 229.73 K. The pressure ratio of the mainstream is 5.36, and the total temperature of the mainstream is 1901.7 K. The total temperature of the secondary stream is 296 K.

2.3. Numerical Method Verification. We applied the numerical simulation method in this study to compare with and verify the results of the jet nozzle wind tunnel test involving the third auxiliary intake valve [16]. As shown in Figure 5, the simulation and experimental results of the static pressure on the tail nozzle are compared. The numerical calculation results were determined to be in good agreement with the experimental results. Therefore, the simulation method adopted in this study can accurately simulate the internal flow characteristics of the ejector nozzle.

2.4. Verification of the Grid Independence. In this study, three sets of grids were defined with grid volumes of 2.2 million, 7 million, and 11 million, corresponding to coarse grid, fine grid, and dense grid, respectively. Figure 6 shows the numerical simulation results of different mesh models, considering the pressure-variation curve along the wall of the tail nozzle as a comparison parameter. The results calculated by the fine and dense grids were very close, with a slight error within 1%. However, the simulation results obtained by the coarse grids were quite different from those obtained by the other two mesh models. Clearly, when the mesh size increased to the fine grid, the simulation calculation results did not depend on the mesh size. Thus, it was more helpful to employ the fine grids for calculations in this study.

3. Result Analysis

The flow inside the ejector nozzle in this study involves the mutual shearing, mixing, and carrying motion of a three-channel flow as well as the mutual interference of the internal and external flows. In particular, at the transonic state,

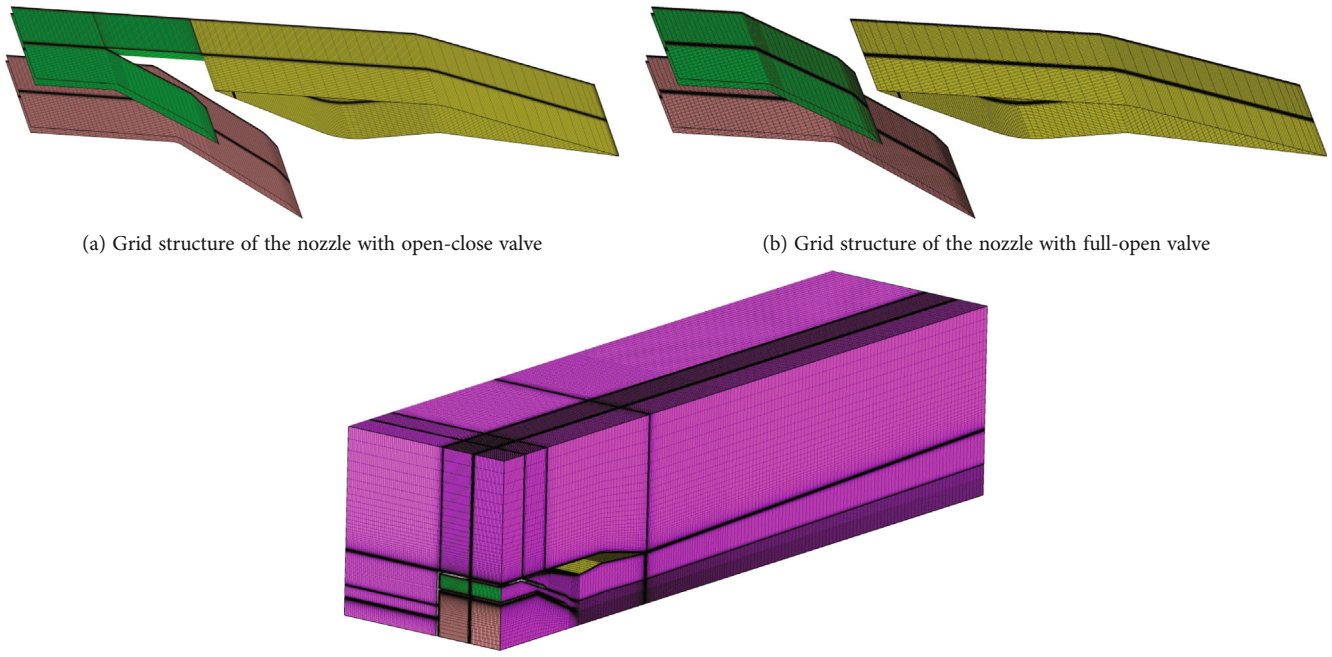

(a) Grid structure of the nozzle with open-close valve

(b) Grid structure of the nozzle with full-open valve

(c) Grid structure of the whole calculation domain

Figure 3: Grid structure of the ejector nozzle model.

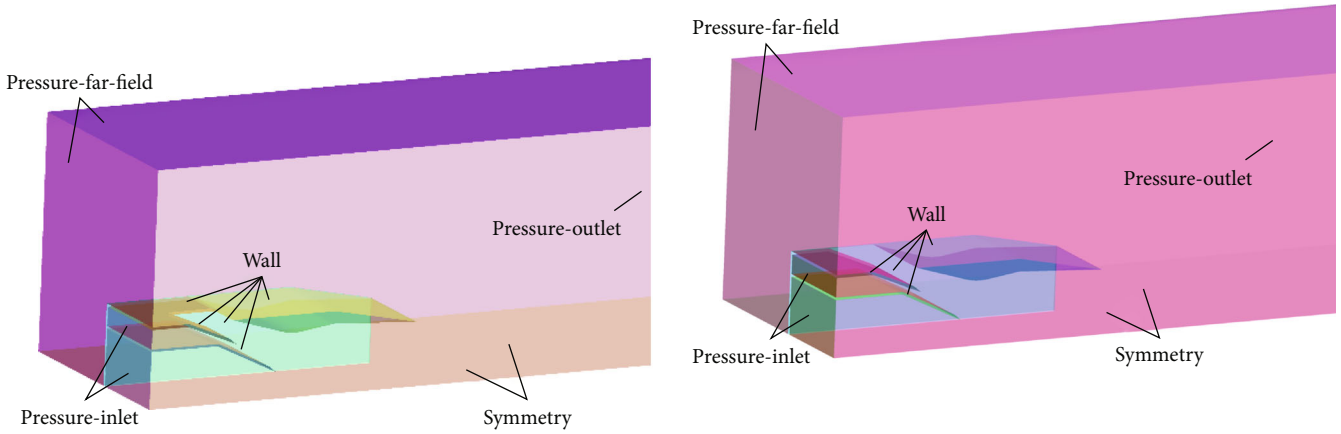

Figure 4: Boundary conditions of the ejector-like nozzle model.

Table 2: Values of the corresponding boundary parameters.

Mach number (M_0)	Environmental pressure (p_0/Pa)	Total temperature ($T_0{}^*/K$)	Pressure ratio of primary flow(NPR_p)	Total temperature of primary flow($T_p{}^*/K$)	Pressure ratio of second flow (NPR_p)	Total temperature of second flow($T_s{}^*/K$)
1.2	30,800	229.73	5.36	1901.7	1.0	296

the coupling strength of the internal and external flows increases. To this end, this study focuses on the following parts: (1) the flow characteristics of the ejector nozzle, (2) the development and characteristics of the vortex inside the nozzle, and (3) the thrust performance of the nozzle. In the next section, we discuss the analyses of these parts in detail.

3.1. Analysis of the Flow Characteristics in the Ejector Nozzle. We first analyze the flow-field structure of the symmetry plane of the two models. Figures 7(a) and 7(b) indicate that the flow-field structures inside two models on the symmetry plane show a high degree of consistency. In the primary flow area, the speed of the primary flow reaches that of sound near the outlet of the contracting primary nozzle and is

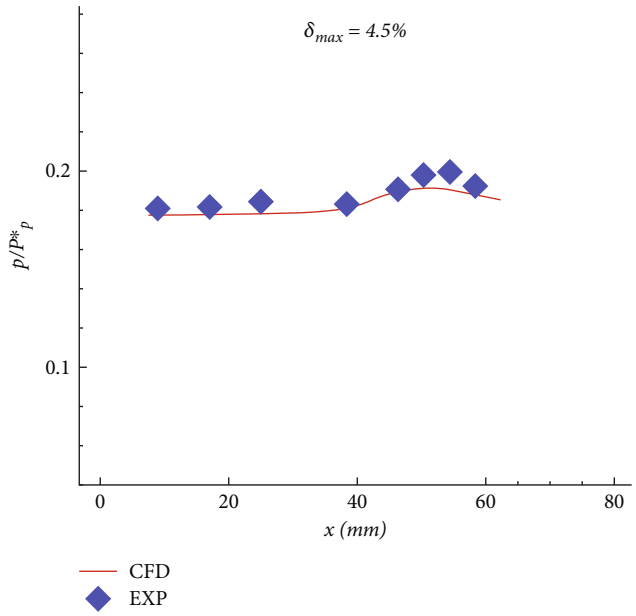

Figure 5: Comparison of the experimental and simulation results (Ma = 1.1).

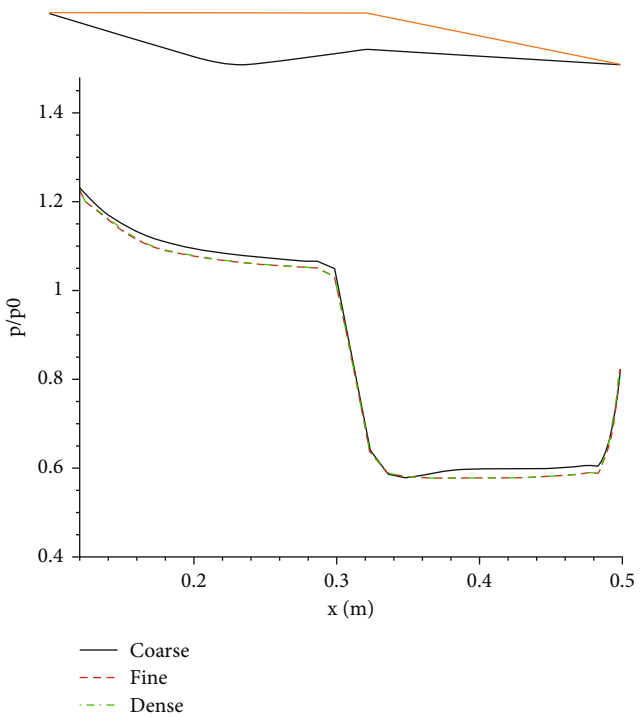

Figure 6: Pressure curves for grid-independence verification.

subsequently increased to supersonic speed by the rapid expansion in the nozzle. At the same time, the air enters the nozzle through the third auxiliary valve and mixes with the secondary flow. Because of the velocity difference between the two flows, shearing and mixing occur, thereby forming a super-subsonic shear layer to transfer energy. Similarly, there is also a speed difference between the mixed flow and the primary flow; thus, the same phenomenon (shearing and mixing) occurs. Subsequently, due to the high primary flow pressure and the weak restriction of the mixed flow on the primary flow, the shear layer formed by the primary flow and the secondary flow gradually approaches the nozzle wall.

There is a large velocity gradient between the primary flow and the secondary flow. With the development of the primary flow, the velocity gradient on both sides decreases, which indicates that the shear layer gradually increases the mechanical energy of the secondary flow fluid during the development process. The secondary flow accelerates the flow in the shrinking circulation space, and obtains energy by mixing with the primary flow and the third auxiliary flow. We mainly focus on the difference of the flow-field structure and shear layer characteristics between the two models. As shown in Figure 7(a), the low pressure near the secondary flow inlet in the nozzle creates a low-pressure environment for the third auxiliary flow, so that the surrounding ambient gas enters the nozzle through the open-close valves. Obviously, a shear layer is formed between the third auxiliary flow and the secondary flow. The secondary and third auxiliary flow jointly suppress the expansion of the primary flow, so that the shear layer of the primary flow cannot adhere to the wall surface of the tail nozzle. The difference compared with Figure 7(b) is that, in Figure 7(a), the secondary flow gas moves more downward and forward, and the flow rate of the third auxiliary flow is more drawn into the nozzle. While in Figure 7(b), part of the secondary flow gas rolls up mixing with the third auxiliary flow and moves downstream. The third auxiliary flow is significantly reduced, which reduces the suppression of the primary flow from the mixed flow of the secondary and third auxiliary flow. On this symmetry plane, the range of the high Mach number region is decreasing, as is the highest internal Mach number.

We monitored nine pressure curves along the wall of the tail nozzle to express the pressure change in the nozzle more clearly. Figure 8 shows the position of the pressure monitoring curves along the tail nozzle. Figures 9(a)–9(i) show the curves of the pressure changes along the trail nozzle. Using the monitoring curve of the nozzle with full-open valve, we can determine the pressure change in the nozzle (taking Figure 9(a) as an example). At the beginning, the curve is located in the influence area of the third auxiliary flow. Because the wall of the tail nozzle bends downward, the air will pass through the throat of the nozzle (point A) and subsequently expand. Then the pressure drops rapidly when it reaches the turning point (point B). This is mainly because before point A, the pressure is mainly affected by the combined action of the secondary and third auxiliary flow. The less stable pressure changes before point A are due to the unstable flow of the secondary and third auxiliary streams. Between point A and point B, the subsonic gas is decelerated and pressurized in this expansion section. Then after point B, the subsonic gas accelerates and decompresses in this constricted section. Therefore, before and after the throat of the nozzle (point A), the airflow undergoes a transition from a forward pressure gradient to a reverse pressure gradient. Near the outlet of the tail nozzle, the pressure of the third auxiliary flow and the ambient pressure gradually reach equilibrium.

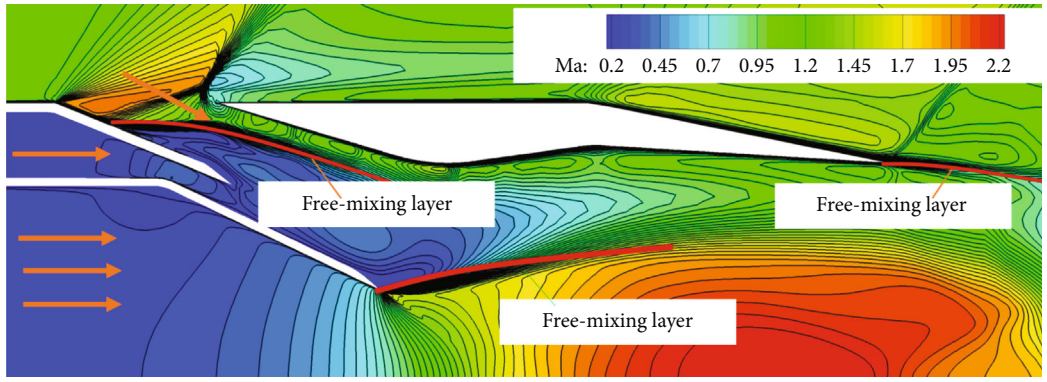

(a) Nozzle with open-close valve

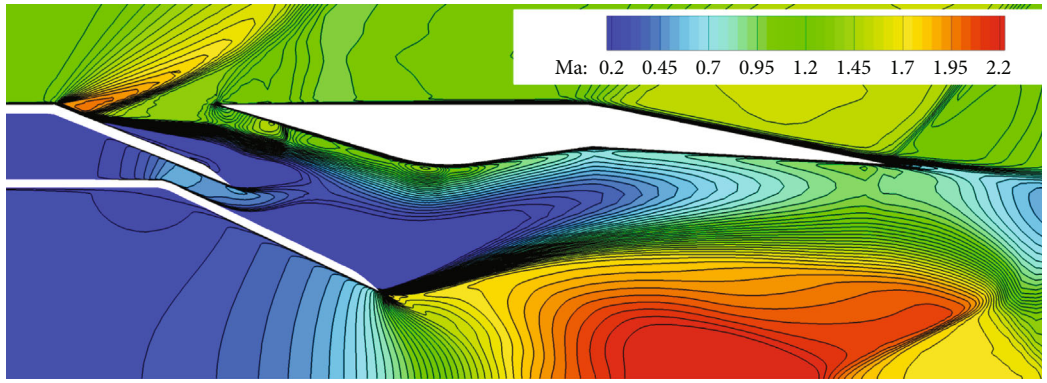

(b) Nozzle with full-open valve

Figure 7: Mach contours of the symmetry plane of the ejector nozzles.

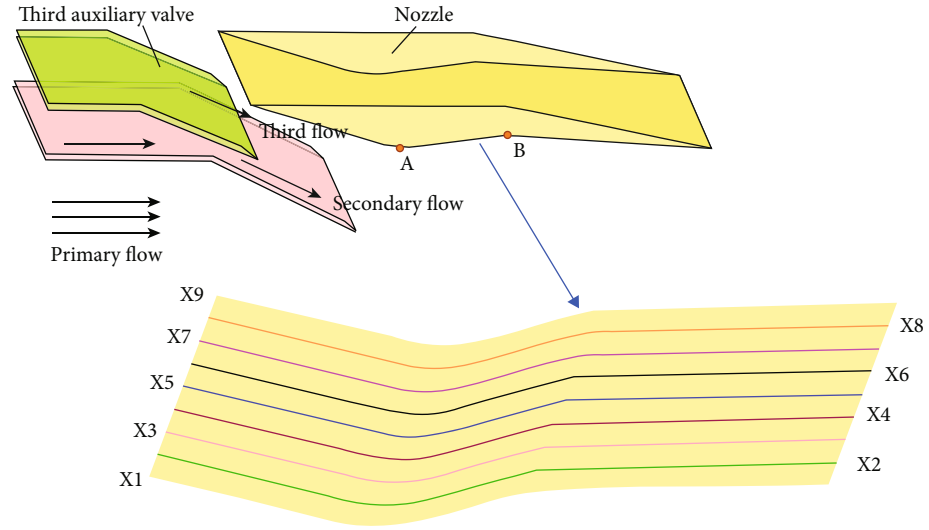

Figure 8: Position of the pressure monitoring curves along the tail nozzle.

The nine figures show that the pressure curves are basically the same in the nozzle with full-open valve, and only two monitoring lines (h and i) differ slightly due to the influence of the side wall. Further, in the nozzle with full-open valve, there is almost no lateral airflow, and the pressure is uniformly distributed along the longitudinal direction. Contrarily, in the nozzle with open-close valve, the pressure changes on each monitoring line are significantly different. On the opening side of the intake valve, the pressure along the path varies significantly. As the monitoring line gradually approaches the side where the valve is closed, the pressure-variation range along the path gradually decreases. All in all, the nine figures show that the pressure in the nozzle is not uniformly distributed along the longitudinal direction, which will inevitably cause the lateral flow of the air, thereby forming vortexes in the nozzle.

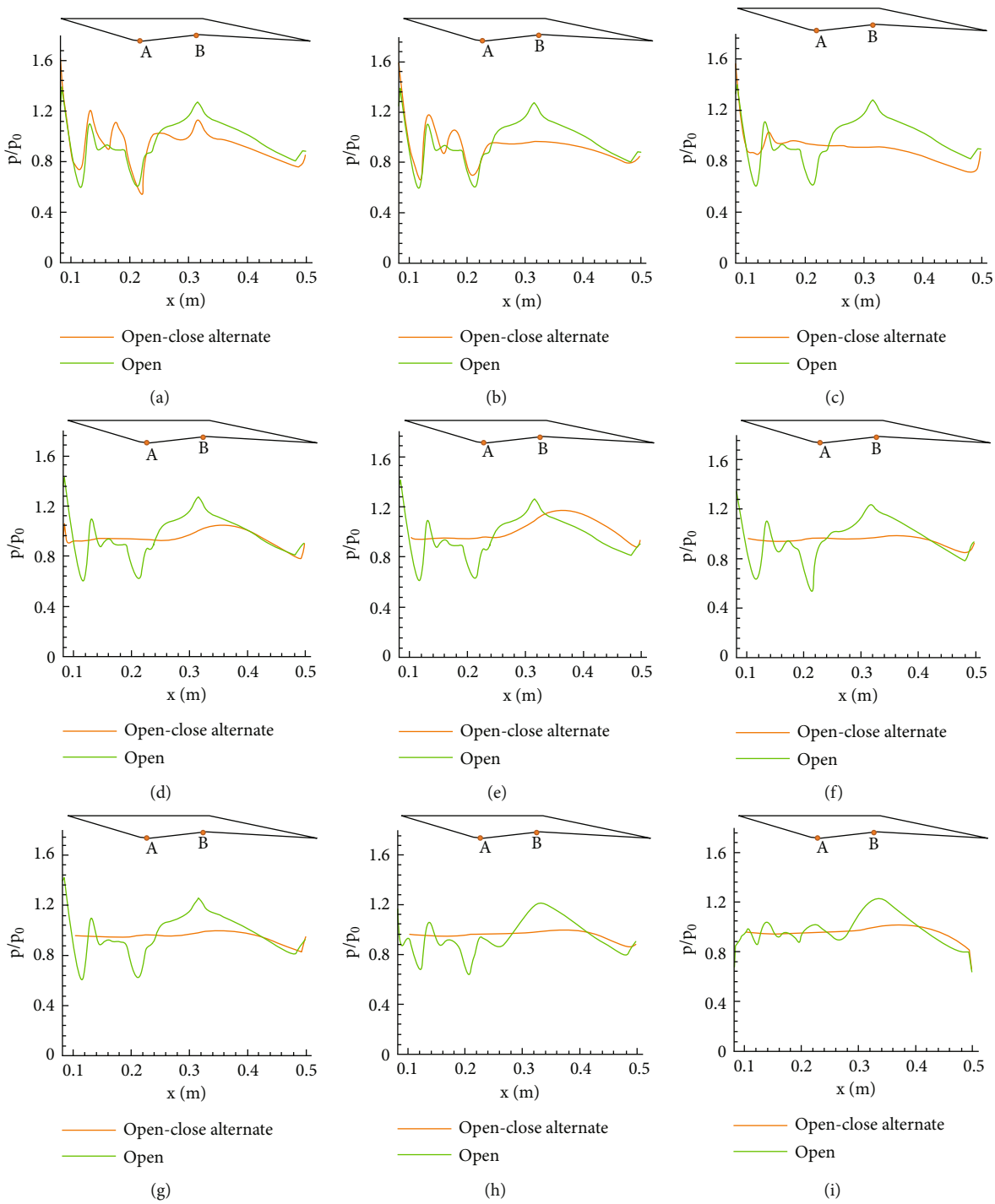

Figure 9: Pressure changes in the monitoring curves along the tail nozzle.

3.2. Comparison of the Characteristics of the Vortex inside the Nozzle. We monitored the vortex development characteristics of five surfaces (a, b, c, d, and e) shown in Figure 10 to more intuitively analyze the vortex development characteristics in the nozzle. Specifically, surface *a* is the throat of the nozzle, surface *b* is the turning point of the nozzle, surfaces *c* and *d* are located at the end of the nozzle, and surface *e* is the outlet of the nozzle. The specific location parameters of the monitoring surface are listed in Table 3. Figures 11–15 show the vortex distribution of the five monitoring surfaces to analyze the flow characteristics in the nozzle.

From Figures 11–15, we observe the phenomenon of lateral flow in the nozzle with open-close valve. Vortexes can be seen on each monitoring surface, and the flow pattern in the tube is complicated. Contrarily, in the nozzle with full-open valve, there is basically no lateral flow phenomenon. That is, there is no vortex on each monitoring surface,

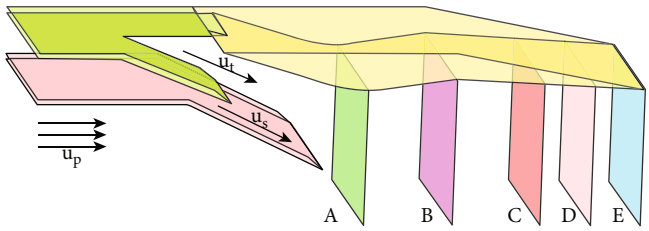

Figure 10: Positions of the monitoring surfaces for the vortexes.

Table 3: Monitoring surface position parameters.

Monitoring surface	Position
a	$X = 226.4$ mm (throat of the nozzle)
b	$X = 313$ mm (turning point of the nozzle)
c	$X = 400$ mm
d	$X = 450$ mm
e	$X = 497$ mm (outlet of the nozzle)

and the flow pattern is relatively simple. Evidently, in the nozzle with open-close valve, the primary flow is affected at the position of the open-close alternation, forming two "semi-circular" structures, whereas the primary flow is quite smooth and basically horizontal in the nozzle with full-open valve.

Figures 11(a) and 11(b) show schematic diagrams of the vortex at monitoring surface *a* (nozzle throat). Because the location of monitoring surface *a* is close to the entrance of the tail, the lower half of the monitoring surface is mainly affected by the state of the mainstream flow, and therefore, it exhibits a high degree of consistency. The mainstream gas flows steadily through the lower half of the monitoring surface in the direction of the flow line, with no lateral flow or air mixing and no vortex generated.

The right side of the monitoring surface is the open valve. The secondary flow passes through here and moves downstream through the tapered channel, forming a low-pressure zone. At the same time, the outside air enters through the third auxiliary valve, resulting in a relatively high Mach number here. In addition, in the nozzle with open-close valve, the vortex rolls up at the right entrance because of the influence of the lateral movement of the third auxiliary flow. However, in the nozzle with full-open valve, the air smoothly enters the nozzle with the Mach number evenly distributed in the upper half of the monitoring surface.

As shown in Figures 12(a) and 12(b), when the airflow moves to monitoring surface *b* (turning point of the nozzle), the flow undergoes a significant change. That is, with the mixing of the primary flow, secondary flow, and third flow in the nozzle, the flow area dominated by the primary flow increases. In particular, in the nozzle with open-close valve, the primary flow is affected at the position of the open-close alternation, forming two "semi-circular" structures with a pair of vortexes generated near the upper wall. With the continuous acceleration of the airflow, the range of $Ma < 1$ keeps decreasing, although the vortex is basically in the range of $Ma < 1$. The direction of the vortex loop flow line points from the center to the outside, and the spiral point is unstable and may scatter at any time. At this time, the flow direction of the vortex loop changes, and a limit cycle structure is formed. In addition, the air moves from the top to the bottom in Figure 12(a) but in the opposite direction in Figure 12(b).

Figures 13–15 show that over time, the airflows merge, increasing the movement complexity. The vortex basically appears as a pair of vortexes throughout its development process, and there is always a pair of fully developed vortexes at the upper right of the cross-section (i.e., at the entrance of the third auxiliary flow). Thus, with the development of the flow field in the nozzle, a pair of relatively weakly developed vortexes will also be generated at the upper left of the cross-section (i.e., where the tertiary flow gate is closed). Moreover, the direction of the airflow gradually changes from bottom-top to top-bottom. The primary flow is always suppressed by the secondary flow and the third auxiliary flow. The primary flow develops fully at the junction of the open-close valve, whereas the remaining positions are strongly restrained by the secondary and third auxiliary flows. This uneven development leads to the development of the vortex in the nozzle. There are two main reasons for the formation of the vortex: one is the lateral flow caused by the open-close valve and the other is the unevenness of the mainstream development.

3.3. Thrust Performance of the Ejector Nozzle. To evaluate the pros and cons of the design of the ejector nozzle of an engine, its thrust performance is the core parameter, and the thrust coefficient is an important index for measuring the thrust performance of the tail nozzle. The nozzle in this study contains three flow paths, and the incoming flow parameters of each flow-path fluid, i.e., the flow parameters in the tube, are different. Therefore, the thrust of each flow-path fluid is also different, and the isentropicity of each flow path should, therefore, be considered separately. The thrust coefficient C_f used in this study is defined as

$$C_{\mathrm{f}} = \frac{F_{\mathrm{a}}}{\sum F_{\mathrm{i}}}, \tag{1}$$

where

$$F_{\mathrm{a}} = F_{\mathrm{v}} + F_{\mathrm{p}}, \tag{2}$$

$$F_{\mathrm{v}} = \dot{m}v, \tag{3}$$

$$F_{\mathrm{p}} = (p_{\mathrm{e}} - p_0)A_{\mathrm{e}}. \tag{4}$$

Among them, F_a represents the actual thrust of the ejector nozzle, which is the sum of the theoretical isentropic thrust of each flow. The actual thrust F_a of the ejector nozzle is composed of momentum thrust F_v and differential pressure thrust F_p. $\dot{m}$ and v represent the ejector nozzle's outlet flow and exit velocity, respectively. The product of the two represents the thrust produced by the fluid momentum. p_e

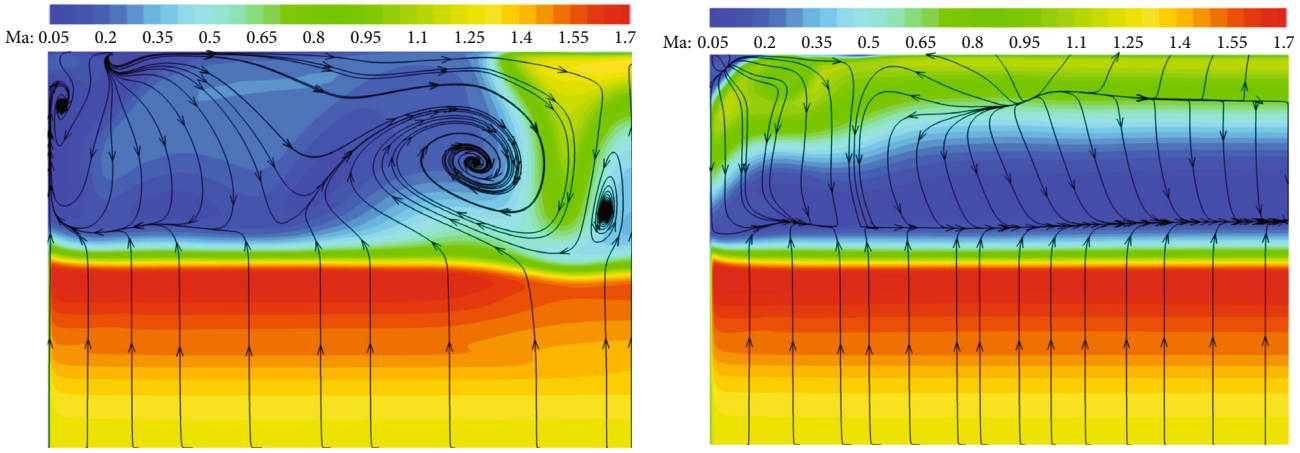

(a) Nozzle with open-close valve (b) Nozzle with full-open valve

Figure 11: Vortex structure of monitoring surface a (throat of the tail nozzle).

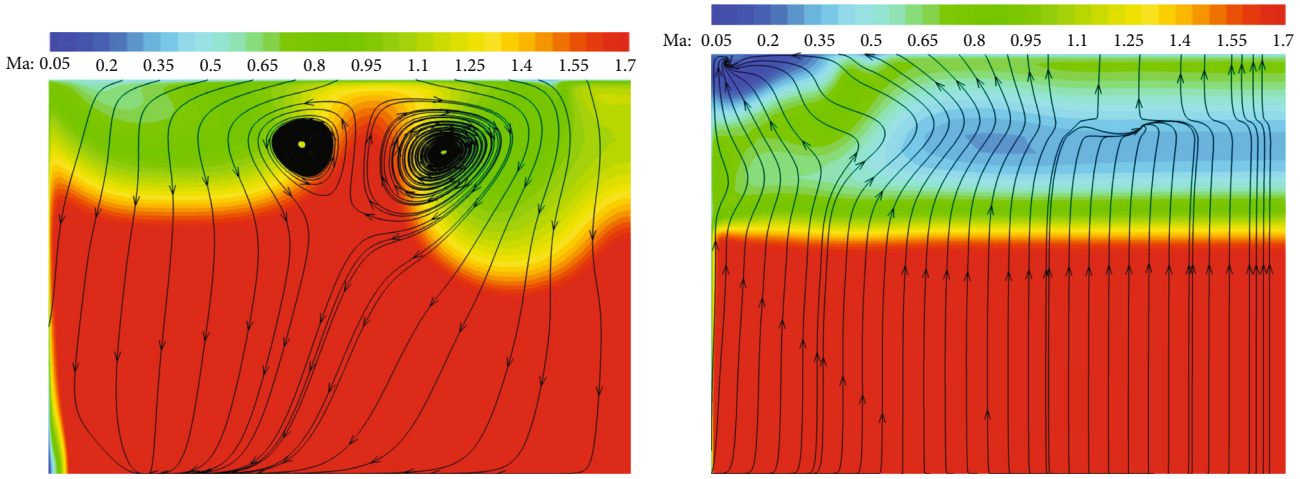

(a) Nozzle with open-close valve (b) Nozzle with full-open valve

Figure 12: Vortex structure of monitoring surface b (turning point of the tail nozzle).

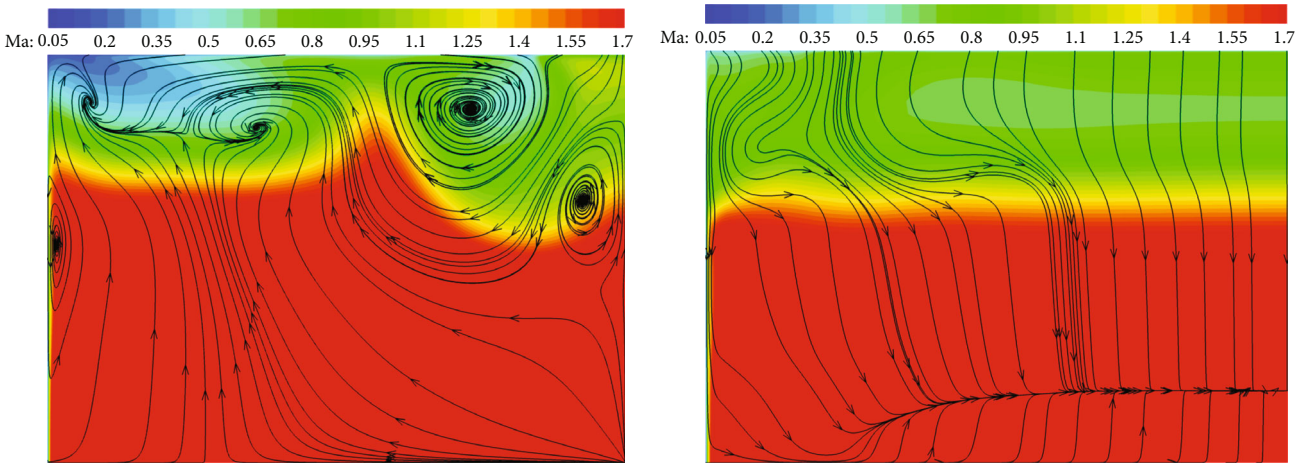

(a) Nozzle with open-close valve (b) Nozzle with full-open valve

Figure 13: Vortex structure of monitoring surface c.

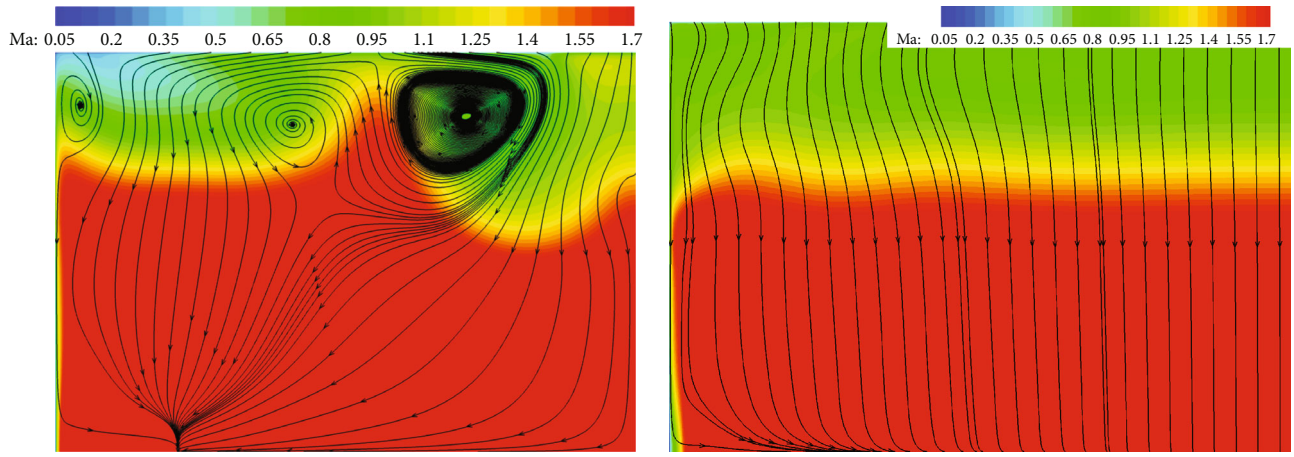

(a) Nozzle with open-close valve (b) Nozzle with full-open valve

Figure 14: Vortex structure of monitoring surface d.

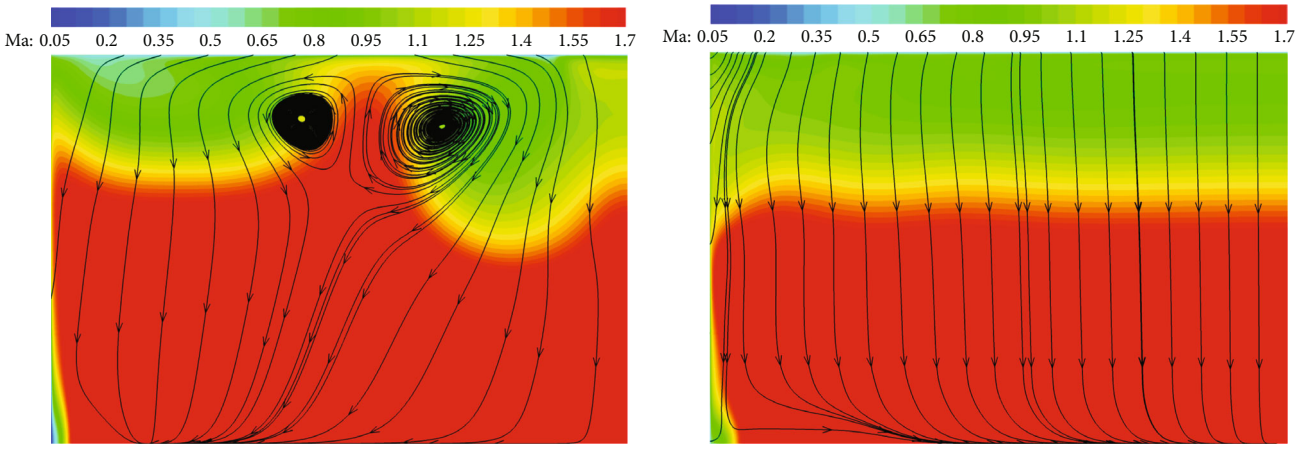

(a) Nozzle with open-close valve (b) Nozzle with full-open valve

Figure 15: Vortex structure of monitoring surface *e* (outlet of the tail nozzle).

represents the static pressure at the exit of the ejector nozzle, p_0 represents the ambient pressure, A_e represents the ejector nozzle's exit area, and F_p represents the thrust generated by the fluid due to expansion.

Table 4 shows the thrust performance comparison of the two models. As can be seen from the table, since the initial conditions of the two models remain consistent, the primary flow rate is the same. However, because of the difference in the structure of the auxiliary intake valve, the third auxiliary flow differs. In the model with open-close valve, the flow rate of the third auxiliary flow is 0.286 kg/s, while 0.567 kg/s for the model with full-open valve. It is precisely because the flow rate of the third auxiliary flow in the model with full-open valve is relatively large, and that a high-pressure environment is generated in the secondary flow area, which inhibits its flow (0.131 kg/s for the model with full-open valve, while 0.223 kg/s for the model with open-close valve). Ultimately, the total flow of the nozzle in two models also differs (2.333 kg/s for the model with full-open valve, while 2.143 kg/s for the model with open-close valve). In addition,

Table 4: Thrust performance parameters of the ejector nozzle under two different working conditions.

State	Open-close valve	Full-open valve
Flow rate of the primary flow (kg/s)	1.63	1.63
Flow rate of the second flow (kg/s)	0.223	0.131
Flow rate of the third auxiliary flow (kg/s)	0.286	0.567
Flow rate of the ejector nozzle (kg/s)	2.143	2.333
Velocity of the ejector nozzle (m/s)	1,048.9	960.0
Static pressure of the ejector nozzle (Pa)	20,834.3	23,984.0
Thrust coefficient	0.698	0.796

the auxiliary intake valve structure also has an effect on the vortex in the flow field. In the nozzle with open-close valve, multiple pairs of vortexes are generated by the lateral flow, which makes the parameters such as velocity and static pressure at the nozzle outlet different from those of the nozzle

with the full-open valve, and this eventually leads to the difference in the thrust coefficient (0.796 for the model with full-open valve, while 0.698 for the nozzle with open-close valve). It can be concluded that under the conditions of this paper, the fully-open auxiliary intake valve structure increases the flow rate of the third auxiliary flow, thereby suppressing the expansion of the primary flow and increasing the thrust performance of the ejector nozzle.

4. Conclusion

In this study, we established two models: the nozzle model with an open-close valve and that with a full-open valve. We contrasted and analyzed the flow-field structures and the development characteristics of vortexes at transonic velocity. The results reveal the following.

(1) A lateral flow occurs inside the nozzle with the open-close valve, and the internal pressure is unevenly distributed in the circumferential direction, thus forming a constantly evolving vortex. However, there is no lateral flow inside the nozzle with the full-open valve, and the internal pressure is evenly distributed in the circumferential direction

(2) The primary flow dominates the internal flow of the ejector nozzle, which expands rapidly in the tube and produces a shear layer structure with the secondary flow

(3) The open-close valve affects the flow characteristics of the secondary flow and the third auxiliary flow, increasing the flow rate of the secondary flow but causing the flow of the third auxiliary flow decreased

(4) In the nozzle with full-open valve, the secondary flow and the third auxiliary flow have a stronger restraint effect on the primary flow, which suppresses the primary flow overexpansion phenomenon with the increase of the thrust coefficient from 0.698 to 0.796

Data Availability

Some or all data, models, or code that support the findings of this study are available from the corresponding author upon reasonable request. All data, models, and code generated or used during the study appear in the submitted article.

Conflicts of Interest

The authors declare that they have no conflicts of interest.

References

[1] A. M. El-Nady, M. Y. M. Ahmed, M. A. El-Senbawy, and A. M. Sarhan, "Experimental and theoretical study on a dual-thrust rocket motor with subsonic intermediate nozzle," *Proceedings of the Institution of Mechanical Engineers, Part G: Journal of Aerospace Engineering*, vol. 232, no. 10, pp. 1844–1852, 2018.

[2] P. H. Pedreira, J. R. Lauretta, and S. D'Hers, "Planar nozzles for controllable microthrusters," *Journal of Aerospace Engineering*, vol. 30, no. 3, 2017.

[3] A. Ferrero and D. Pastrone, "Plasma actuator–assisted rocket nozzle for improved launcher performance," *AIAA Journal*, vol. 57, no. 4, pp. 1348–1354, 2019.

[4] J. Hoffman, "A general method for determining optimum thrust nozzle contours for chemically reacting gas flows," *AIAA Journal*, vol. 5, no. 4, pp. 670–676, 1967.

[5] D. Davis and R. Abel, "The effects of internal nozzle contouring on nozzle performance," in *19th Joint Propulsion Conference*, Seattle, WA, USA, 1983.

[6] P. Storm and M. Cappelli, "LIF characterization of arcjet nozzle flows," in *32nd Joint Propulsion Conference and Exhibit*, Lake Buena Vista, FL, USA, 1996.

[7] T. Galambos, "A CFD analysis of a scarfed plugged nozzle to determine nozzle loadsduring ignition," in *26th Joint Propulsion Conference*, Orlando, FL, USA, 2013.

[8] M. Ferlauto, A. Ferrero, and R. Marsilio, "Fluidic thrust vectoring for annular aerospike nozzle," in *AIAA Propulsion and Energy 2020 Forum*, Washington, DC, 2020.

[9] M. F. Osborn, T. D. Holman, D. A. Rosenberg, S. G. Tuttle, and L. T. Williams, "Overcoming low nozzle efficiency: a test-correlated numerical investigation of low Reynolds number micro-nozzle flow," in *51st AIAA/SAE/ASEE Joint Propulsion Conference*, Orlando, FL, 2015.

[10] A. N. Rao, A. Kushari, and G. K. Jaiswal, "Effect of nozzle geometry on flowfield for high subsonic jets," *Journal of Propulsion and Power*, vol. 34, no. 6, pp. 1596–1608, 2018.

[11] A. J. Harroun, S. D. Heister, and J. H. Ruf, "Computational and experimental study of nozzle performance for rotating detonation rocket engines," *Journal of Propulsion and Power*, vol. 37, pp. 660–673, 2021.

[12] T. Luginsland, "How the nozzle geometry impacts vortex breakdown in compressible swirling-jet flows," *AIAA Journal*, vol. 53, no. 10, pp. 2936–2950, 2015.

[13] W. Da and D. Zhen-ning, "Research on pneumatic adjustable nozzle," *Propulsion Technology*, vol. 7, no. 6, pp. 31–37, 1986.

[14] W. Da and D. Zhen-ning, "Performance analysis of pneumatic regulating nozzle," *Acta Automatica Sinica*, vol. 6, no. 6, pp. 256–261, 1987.

[15] W. Deng, Y. Dai, and J. Wang, *Numerical Investigation on Mass-Flow and Thrust Performance of the Ejector-Nozzle*, Aeronautical Science & Technology, 2014.

[16] Z. Wei-yang, *Computational and Experimental Study on a Variable Nozzle for TBCC with Tandem Layout*, Nanjing University of Aeronautics and Astronautics, 2012.